Chinese Physics B



# Evidence for magnetic order in the transverse field Ising magnet $TmZn_2GaO_5$

To cite this article before publication: Guangkai Zhang *et al* 2025 *Chinese Phys. B* in press https://doi.org/10.1088/1674-1056/ae2bee

# Evidence for magnetic order in the transverse field Ising magnet $TmZn_2GaO_5$

Guangkai Zhang,[1,2] Xubin Ye,[2] Maocai Pi,[2,3] Jie Zhang,[2,3] Shuai Tang,[2,3] Chao Chen,[2] Mengqi Ye,[2] Zhao Pan,[2,3] Xiaomei Qin,[1,*] Youwen Long,[2,3,†] and Yao Shen[2,3,‡]

[1] *Department of Physics, Shanghai Normal University, Shanghai 200234, China*
[2] *Beijing National Laboratory for Condensed Matter Physics, Institute of Physics, Chinese Academy of Sciences, Beijing 100190, China*
[3] *School of Physical Sciences, University of Chinese Academy of Sciences, Beijing 100049, China*

(Dated: November 25, 2025)

It has been theoretically predicted that the transverse-field Ising model on a triangular lattice undergoes two successive Berezinskii-Kosterlitz-Thouless (BKT) phase transitions into an ordered clock phase, separated by an intermediate quasi-long-range BKT phase. Experimentally, while this model has been realized in $TmMgGaO_4$, studies of BKT physics in this material have been hindered by structural disorder caused by random Mg/Ga substitution in the intercalated layers. To address this challenge, we successfully synthesized a new frustrated antiferromagnet $TmZn_2GaO_5$, which preserves the triangular-lattice structure but features an ordered Zn/Ga configuration, thereby eliminating structural disorder. Magnetic susceptibility and heat capacity measurements confirm the experimental realization of the transverse-field Ising model. Although no hint of phase transition is observed at zero field, specific heat measurements under longitudinal magnetic fields reveal a weak anomaly near 0.3 K, indicating magnetic ordering. The resulting phase diagram aligns with theoretical predictions whereby the zero-field BKT transitions, undetectable in heat capacity, are replaced by conventional ones under magnetic fields. Our results establish $TmZn_2GaO_5$ as a new platform for studying BKT physics in quantum materials.

PACS numbers: 75.10.Jm; 75.30.Cr; 75.30.Gw; 75.40.-s; 82.75.Fq

## INTRODUCTION

Rare-earth magnets have emerged as a promising platform for studying quantum magnetism due to their highly tunable ground state and spin anisotropy, arising from the interplay of strong spin-orbit coupling, crystal electric field (CEF) splitting, and complex magnetic interactions. For instance, $Yb^{3+}$, a Kramers ion with an odd number of $4f$ electrons, typically exhibits a symmetry-protected Kramers doublet CEF ground state with enhanced quantum fluctuations, which, combined with strong geometric frustration, can potentially stabilize an exotic quantum disordered state termed quantum spin liquid (QSL) [1–3]. Great efforts have been made in the experimental exploration of this state in triangular-lattice materials, leading to the discovery of QSL candidates such as $YbMgGaO_4$ [4–8], $NaYbSe_2$ [9, 10], and $YbZn_2GaO_5$ [11–13]. Meanwhile, QSL states are also proposed for $Ce^{3+}$-based pyrochlore magnets, another Kramers ion possessing a doublet ground state, such as $Ce_2X_2O_7$ ($X$=Sn, Zr, Hf) [14–19]. Here, however, the situation is more complex as the $Ce^{3+}$ doublet ground state exhibits a distinctive dipole-octupole character, leading to a phase diagram that potentially hosts multiple types of QSL states.

In contrast, non-Kramers ions with an even number of electrons often exhibit a non-Kramers doublet ground state — either magnetic or nonmagnetic [20] — or more commonly, a nonmagnetic singlet state [21]. However, in rare cases, if the energy gap between the singlet ground state and excited states is comparable to magnetic interactions, these states may mix and induce magnetic order. Such is the case for the triangular-lattice compound $TmMgGaO_4$, where two low-lying singlet CEF states of $Tm^{3+}$ are separated by a small energy gap, forming a quasi-doublet ground state [22–27]. Moreover, the unique wavefunctions of the quasi-doublet promote strong easy-axis anisotropy, and the CEF gap can be mapped into an effective transverse field, enabling quantum tunneling between the two singlets [23, 28]. Consequently, the magnetism in $TmMgGaO_4$ is well-described by the transverse field Ising model (TFIM) on a triangular lattice. Notably, the transverse field in this material is intrinsic, originating from CEF splitting rather than an external source.

Intriguingly, theoretical studies predict a highly unconventional magnetic phase diagram for the triangular-lattice TFIM. Cooling from the high-temperature paramagnetic phase, the system is expected to first enter a quasi-long-range Berezinskii-Kosterlitz-Thouless (BKT) phase via an upper BKT transition, followed by a lower BKT transition into a three-sublattice ordered clock phase [29–32]. Under longitudinal magnetic fields, both BKT transitions and the intermediate BKT phase are rapidly suppressed, giving way to conventional magnetic transitions and a quantum-fluctuation-stabilized quasi-plateau phase [24, 28, 33], before ultimately reaching a polarized state at high fields [Fig. 1]. While BKT transitions in the originally proposed $XY$ systems are ob-

* xmqin@shnu.edu.cn
† ywlong@iphy.ac.cn
‡ yshen@iphy.ac.cn

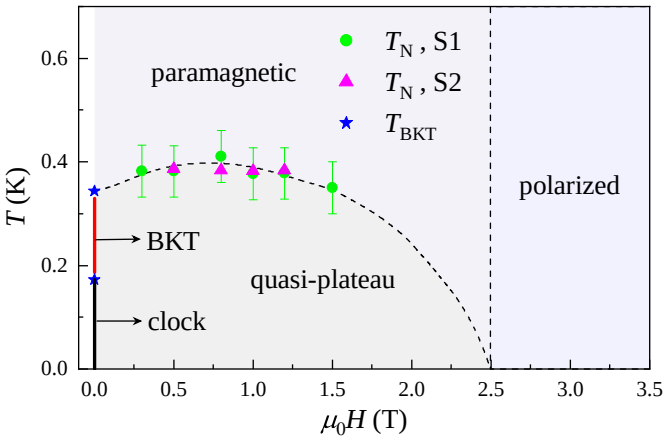


FIG. 1. Magnetic field dependent phase diagram of $TmZn_2GaO_5$. The Néel temperatures $T_N$ are determined from heat capacity measurements of Sample 1 (S1) and Sample 2 (S2), and stars mark the anticipated Berezinskii-Kosterlitz-Thouless (BKT) transition temperatures ($T_{BKT}$). The red and black solid lines indicate the zero-field intermediate BKT phase and clock phase, respectively, and the dashed lines are guides for the eye. The anticipated BKT transition temperatures in the phase diagram were estimated by extrapolating the field-induced phase transition data points.

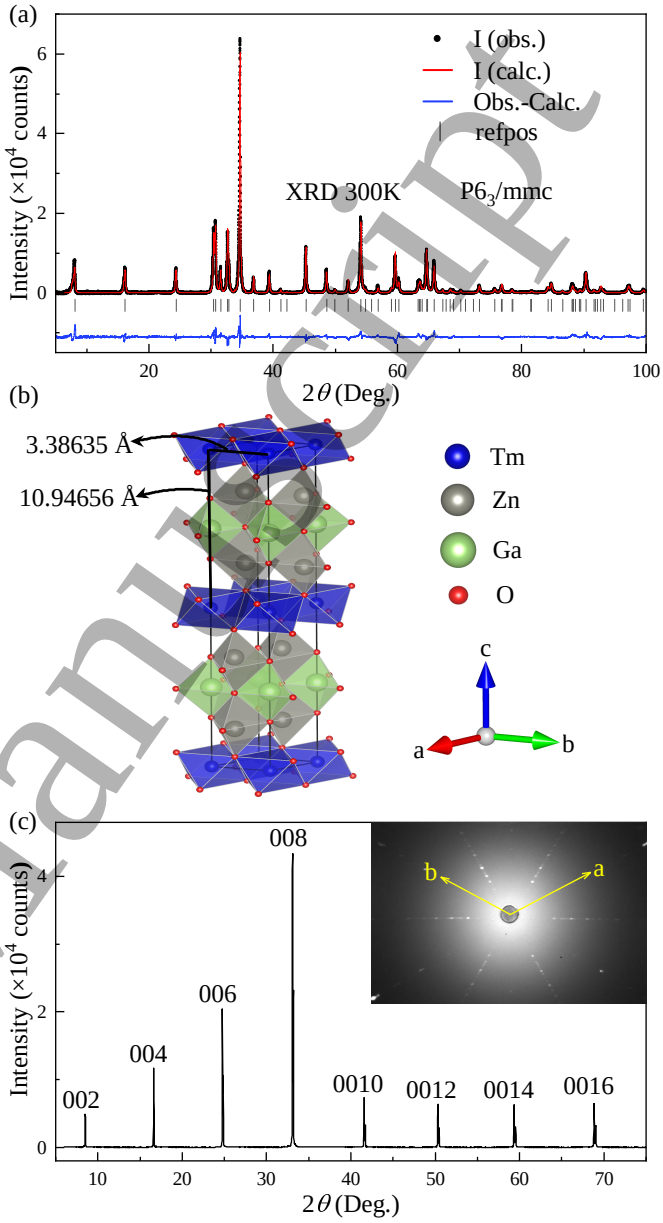


FIG. 2. Crystal structure of $TmZn_2GaO_5$. (a) X-ray powder diffraction pattern collected at room temperature and the corresponding structure refinement results. The observed (obs., black dots), calculated (calc., red line), and difference ($I_{obs.}$-$I_{calc.}$, blue line) profiles are shown. The green ticks indicate the allowed Bragg reflections (refpos). (b) Sketch of the refined $TmZn_2GaO_5$ crystal structure. (c) X-ray diffraction (XRD) profile of a $TmZn_2GaO_5$ single crystal. The inset shows the Laue pattern viewed from the $c$ axis with the lattice $a$ and $b$ directions highlighted.

scured by interlayer coupling, the TFIM offers a pristine platform for exploring BKT physics in quantum magnets. Experimentally, three-sublattice magnetic order has been confirmed in $TmMgGaO_4$ at low temperatures [23, 24], and nuclear magnetic resonance (NMR) measurements indicate a gapless intermediate state [26], suggestive of the proposed BKT phase. However, the obtained field-dependent phase diagram deviates from the quantum Monte Carlo simulations, and the zero-field susceptibility divergence is less pronounced than theoretically predicted [31, 33]. These discrepancies are likely attributable to structural disorder in $TmMgGaO_4$, where Mg and Ga atoms are randomly mixed on symmetry-equivalent sites, obscuring the intrinsic BKT physics. Consequently, the existence of BKT transitions and BKT phases in triangular-lattice TFIM remains an open question.

In this paper, we report the single-crystal synthesis, magnetic properties, and thermodynamic characterization of a newly found triangular-lattice rare-earth antiferromagnet $TmZn_2GaO_5$. Detailed X-ray diffraction (XRD) refinement confirms the absence of structural disorder in this material and the formation of a quasi-two-dimensional (2D) triangular lattice. Combined magnetization and heat capacity measurements reveal a quasi-doublet CEF ground state, comprising two singlets separated by a small energy gap, and exhibiting pronounced easy-axis anisotropy. Thus, its low-energy magnetism is well captured by the TFIM on the triangular lattice. Furthermore, low-temperature heat capacity measurements under external magnetic fields applied along the $c$ axis reveal subtle anomalies indicative of magnetic phase transitions. The resulting field-dependent phase diagram suggests that $TmZn_2GaO_5$ could potentially host BKT phase transitions and the exotic BKT phase.

TABLE I. Refinement parameters of $TmZn_2GaO_5$ X-ray powder diffraction data collected at 300 K. Note that the elevated $\chi^2$ value in the refinement stems from the high intensity of our diffraction peaks, and $R_{wp}$ presents a more appropriate indicator of fit quality here.

| Space group: $P6_3/mmc$ (No.194) | | | | | | |
|---|---|---|---|---|---|---|
| $a = b = 3.38635(2)$ Å, $c = 21.8931(2)$ Å | | | | | | |
| $\alpha = \beta = 90°$, $\gamma = 120°$ | | | | | | |
| Atom | Site | $x$ (Å) | $y$ (Å) | $z$ (Å) | $U$ | Occ. |
| Tm | $2a$ | 0 | 0 | 1/2 | 1.7(1) | 1.01(1) |
| Ga | $2b$ | 0 | 0 | 3/4 | 0.5(1) | 1.00(1) |
| Zn | $4f$ | 2/3 | 1/3 | 0.6378(1) | 0.3(1) | 1.00(1) |
| O1 | $4f$ | 2/3 | 1/3 | 0.5577(2) | 1.6(2) | 1.01(1) |
| O2 | $2c$ | -1/3 | -2/3 | 3/4 | 4.3(3) | 0.97(1) |
| O3 | $4e$ | 0 | 0 | 0.6586(2) | 5.9(2) | 1.02(1) |
| $\chi^2 = 12.27$; $R_{wp} = 5.80\%$; $R_p = 4.03\%$ | | | | | | |

## METHODS

Polycrystalline $TmZn_2GaO_5$ and related samples were synthesized via the solid-state reaction method. Stoichiometric amounts of high-purity (>99.9%) $Tm_2O_3$, $Ga_2O_3$, and ZnO with 10% excess ZnO were thoroughly ground in an agate mortar, pressed into pellets, and calcined at 1350°C in air for 6 hours, with an intermediate grinding. To grow single crystals, the obtained polycrystalline $TmZn_2GaO_5$ samples were thoroughly mixed with ∼5% excess ZnO, packed into latex tubes, and hydrostatically pressed at 300 MPa into rods with ∼6 mm in diameter and ∼10 cm in length. These rods were further sintered at 1350°C in air for 1 hour. Single crystals were then grown using a two-mirror optical floating-zone furnace under a 5-bar oxygen atmosphere, yielding millimeter-sized, high-quality crystals with a growth rate of 1.1 mm/h.

XRD measurements were performed using Huber and Bruker X-ray devices (Cu $K_\alpha$). The Laue photos were taken by a Photonic Sciences Laue camera in backscattering mode with the incident beam along the $c$ axis. The magnetic susceptibility was measured with a SQUID magnetometer (Quantum Design, MPMS 5). The magnetization and heat capacity were measured using a Quantum Design physical property measurement system (PPMS-9T) equipped with a dilution refrigerator insert.

## RESULTS

Figure 2(a) presents the powder XRD pattern of ground $TmZn_2GaO_5$ single crystals. All peaks can be indexed by the $P6_3/mmc$ space group with no detectable impurities. The crystal structure was determined by Rietveld refinement method using the GSAS program, the results of which are presented in Fig. 2(b) and Table I. The structure features $Tm^{3+}$ ions caged in trigonally distorted octahedra, forming triangular layers separated by nonmagnetic $Zn/GaO_6$ blocks, resulting in a quasi-2D architecture. Critically, Zn and Ga atoms occupy distinct Wyckoff positions in an ordered configuration, and incorporating Zn/Ga site mixing does not yield improved refinement results. This eliminates the structural disorder present in $TmMgGaO_4$ caused by random Mg/Ga occupation. Note that neutron diffraction measurements on the isostructual $YbZn_2GaO_5$ show no evidence of Zn/Ga antisite disorder either [11]. Figure 2(c) displays the single-crystal XRD profiles, exhibiting a series of Bragg reflections along the $c$-axis, indicating an $ab$-plane cleavage surface. The sample quality is further validated by Laue diffraction, in which well-defined sharp Laue spots are observed [Fig. 2(c) inset].

Having established the absence of structural disorder in $TmZn_2GaO_5$, we now examine its magnetic properties. Figure 3(a) displays the magnetic susceptibility of $TmZn_2GaO_5$ single crystals with magnetic fields applied parallel and perpendicular to the $c$-axis. The absence of anomaly or divergence between the zero-field cooling (ZFC) and field cooling (FC) curves indicates no magnetic ordering down to 2 K. Below 60 K, the $c$-axis susceptibility follows Curie-Weiss (CW) behavior, and the fitting of the inverse susceptibility yields an CW temperature $\theta_{CW} = -18.51$ K, suggesting dominant antiferromagnetic interactions. The susceptibility deviates from CW behavior above ∼100 K due to the influence of high-energy CEF states at around 40 meV and above [34]. Note that five singlets and four doublets are expected in total for $Tm^{3+}$ in the $D_{3d}$ point group [34, 35]. In sharp contrast, the susceptibility is strongly suppressed for fields perpendicular to the $c$ axis, revealing significant easy-axis anisotropy with the easy axis parallel to the $c$ direction [Fig. 3(a)].

This Ising-type anisotropy is further evidenced in field-dependent magnetization, in which $c$-axis magnetization increases rapidly with field and becomes saturated above ∼8.5 T with a saturation moment of 5.82(1) $\mu_B$/Tm, slightly smaller than that of $TmMgGaO_4$ [23], while in-plane magnetization remains negligible [Fig. 3(b)]. The large saturation moment indicates dominant $|J = 6,\ J_z = \pm 6\rangle$ contributions to the quasi-doublet CEF ground state wavefunction. Notably, the $c$-axis magnetization exhibits non-linear behavior near 1.5 T, which is more clearly visible in its first derivative [Fig. 3(b) inset]. This feature suggests the formation of a field-induced intermediate state, the quasi-plateau phase, which will be discussed subsequently.

To further determine the CEF ground state for the system, we performed detailed heat capacity measurements on $TmZn_2GaO_5$ single crystals. Figure 4(a) shows the temperature-dependent heat capacity in zero field, along with the isostructural nonmagnetic $LuZn_2GaO_5$ data taken as a reference for phonon contributions. After subtracting these phonon contributions, the obtained $TmZn_2GaO_5$ magnetic heat capacity $C_M$ exhibits a broad

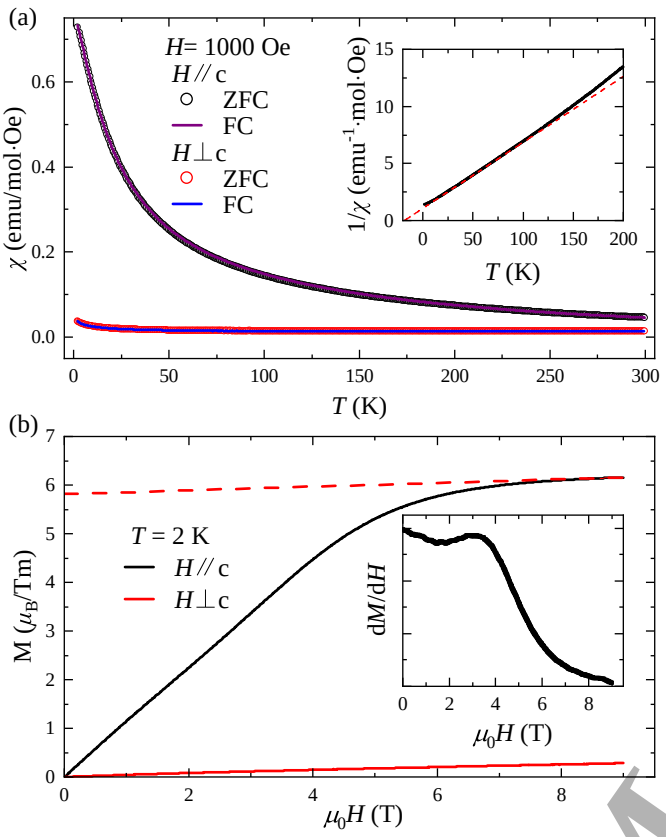


FIG. 3. Magnetic properties of $TmZn_2GaO_5$ single crystals. (a) Magnetic susceptibility measured with a magnetic field of 1000 Oe applied parallel and perpendicular to the $c$ axis. No anomaly or divergence between the zero-field cooling (ZFC) and field cooling (FC) modes can be observed down to 2 K. The inset shows the inverse ZFC profile along the $c$ axis with the red dashed line indicating the Curie-Weiss fit, which deviates from the data above 100 K due to the influence of higher energy CEF states. (b) Isothermal magnetization measured at $T = 2$ K. The dashed line is a linear fit of magnetization above 8.5 T, yielding a saturation moment of 5.82(1) $\mu_B$/Tm (interception), and Van-Vleck susceptibility of $3.8(1)\times10^{-2}$ $\mu_B$/T/Tm (slope). The inset shows the first derivative of magnetization ($dM/dH$) for fields applied along the $c$ axis.

peak below 5 K [Fig. 4(b)], indicating gradual magnetic entropy release without any observable sharp anomaly. This energy scale is much lower than that of the magnetic interactions indicated by the CW temperature ($\theta_{CW}$ = -18.51 K), highlighting the intrinsic geometric frustration of the system. By integrating $C_M/T$, we yield the corresponding magnetic entropy, which accounts for $\sim R\ln 2$ by 30 K, indicating a doublet ground state (effective spin-1/2) well separated from higher energy CEF states [Fig. 4(b)]. Meanwhile, we synthesized polycrystalline $Tm_{0.05}Lu_{0.95}Zn_2GaO_5$, where magnetic interactions are negligible due to extreme dilution. Its heat capacity shows a Schottky-anomaly-like peak centered near 2.5 K [Fig. 4(c)], highlighting the finite splitting within the doublet, as heat capacity would diverge at low temperatures for a degenerate doublet [25]. This observation confirms that the $TmZn_2GaO_5$ ground state is a quasi-doublet composed of two closely spaced singlets. Furthermore, the heat capacity of $Tm_{0.05}Lu_{0.95}Zn_2GaO_5$ can be well described by a two-level system, the fitting of which yields a gap of $\Delta \approx 8.1$ K [Fig. 4(c)], which directly reflects the transverse field magnitude. A more accurate value can be obtained through inelastic neutron scattering. Note that both the magnitude of the saturation moment and the effective transverse field are determined by crystal field splitting, and they are generally independent of each other.

Returning to the $TmZn_2GaO_5$ heat capacity, upon applying a longitudinal magnetic field along the $c$ axis, the broad peak shifts to higher temperatures with increasing field [Fig. 4(d)], confirming its magnetic origin. Focusing on the low-temperature regime, we find no evidence of phase transition down to 0.1 K in zero field [Fig. 4(e)]. A slight upturn emerges below ~0.15 K, characteristic of a nuclear Schottky contribution. Remarkably, under a longitudinal field of 0.3 T, a weak anomaly appears near 0.3 K [Fig. 4(e)], indicating the emergence of a magnetic phase transition. As the field increases, the transition temperature is almost unchanged, ruling out the possibility of a Schottky anomaly, which is expected to shift to higher temperatures with increasing field. At ~1.5 T, it merges with the nuclear Schottky anomaly, and at higher fields, the phase transition becomes indistinguishable within the dominant nuclear Schottky anomaly. To verify the presence of field-induced phase transitions, we performed replicate measurements on a second $TmZn_2GaO_5$ single crystal, observing consistent heat capacity anomalies [Fig. 4(f)]. These results are summarized in the field-dependent phase diagram shown in Fig. 1.

## DISCUSSIONS

Our combined magnetic properties and heat capacity measurements establish that the $TmZn_2GaO_5$ ground state is a quasi-doublet, consisting of two singlets separated by a small energy gap, exhibiting strong easy-axis anisotropy. This system is therefore well-described by the TFIM on a triangular lattice. Within this framework, the competition between the transverse field and magnetic interactions dictates distinct ground states. If the transverse field dominates, the system enters a polarized state effectively described as a nonmagnetic singlet, as in $KTmSe_2$ [36]. In another aspect, with stronger magnetic interactions, the system favors either a stripe phase (with significant next-nearest-neighbor coupling) or a three-sublattice clock phase (as in $TmMgGaO_4$ [23]). For $TmZn_2GaO_5$, the observed field-dependent phase diagram aligns most closely with the clock phase scenario. In this case, the zero-field magnetic ground state is a clock phase, separated from the high-temperature para-

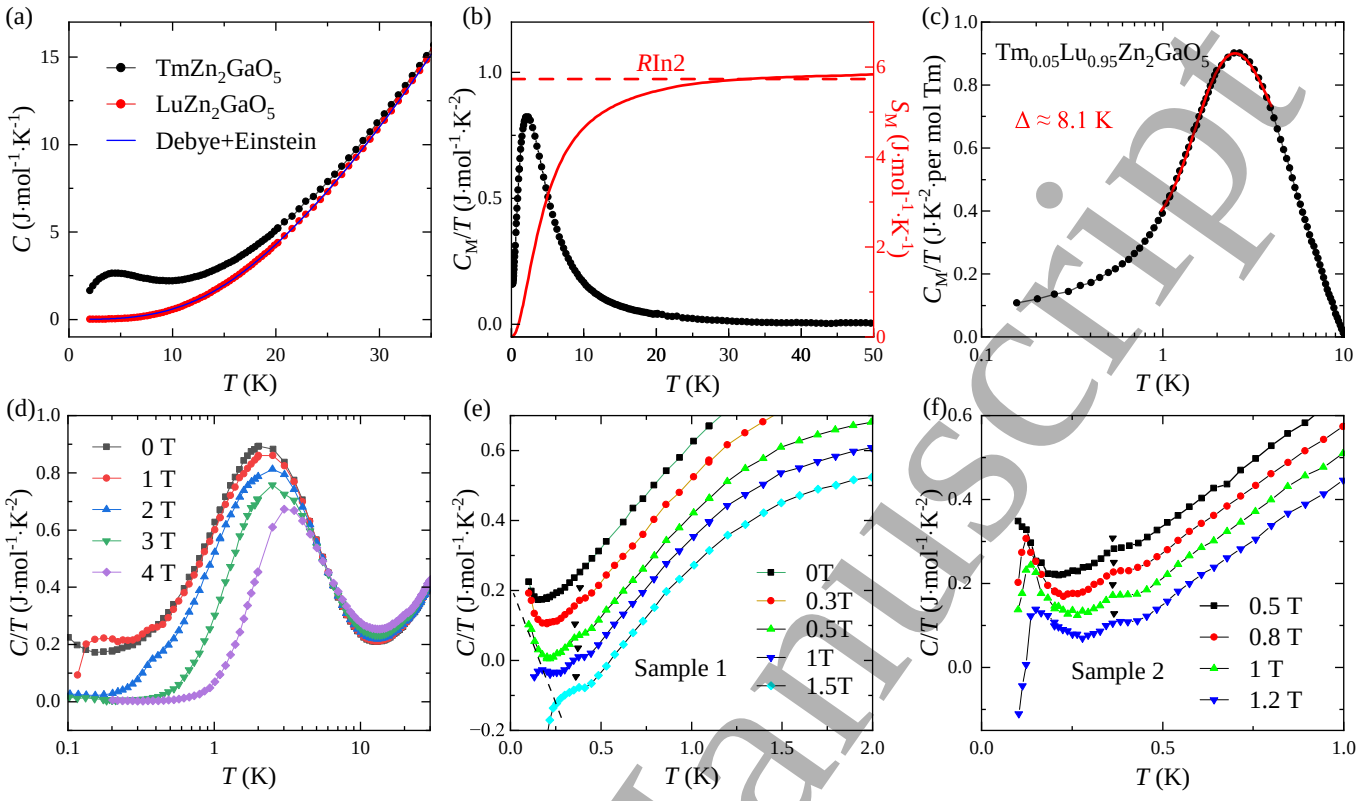


FIG. 4. Heat capacity of $TmZn_2GaO_5$ single crystals. (a) Zero-field heat capacity of $TmZn_2GaO_5$, compared with polycrystalline nonmagnetic $LuZn_2GaO_5$, serving as the phonon reference, which can be well fitted by the Debye–Einstein equation. (b) Magnetic heat capacity $C_M$ of $TmZn_2GaO_5$ obtained by subtracting phonon contributions. The magnetic entropy is calculated through $S(T) = \int_0^T C_M(T)/TdT$. The dashed line indicates $R\ln 2$ on the right axis, where $R$ is the gas constant. (c) Zero-field heat capacity of diluted polycrystalline $Tm_{0.05}Lu_{0.95}Zn_2GaO_5$. The red solid line represents a fit to a two-level system with a gap of $\Delta \approx 8.1$ K. (d) Temperature-dependent heat capacity measured under the indicated magnetic fields applied along the $c$ direction. (e), (f) Low temperature heat capacity for two $TmZn_2GaO_5$ single crystals (Sample 1 and Sample 2). Curves are vertically offset for clarity. Triangles mark the magnetic phase transitions, which merge with the nuclear Schottky anomaly (dashed line) near 1.5 T.

magnetic state by two successive BKT transitions and an intermediate BKT phase [Fig. 1]. Note that such BKT transitions are expected to leave no resolvable heat capacity signature [37]. Applying longitudinal magnetic fields suppresses these BKT transitions. Instead, conventional magnetic transitions emerge, manifested as the heat capacity anomalies [Fig. 4(e), (f)]. Meanwhile, the clock phase and the BKT phase are replaced by a quasi-plateau phase, a two-up-one-down plateau phase dressed with quantum fluctuations [28], which is further indicated by the non-linear magnetization we observe [Fig. 3(b)]. Ultimately, under sufficiently high fields, the system enters a field-induced polarized state.

It is insightful to compare the parameters between $TmZn_2GaO_5$ and $TmMgGaO_4$. The CW temperature of $TmZn_2GaO_5$ ($\theta_{CW} = -18.51$ K) is comparable to that of $TmMgGaO_4$ ($\theta_{CW} = -19.1$ K [23]), indicating similar exchange interaction strength. In contrast, the effective transverse field, which can be inferred from the heat capacity of dilute samples, is larger in $TmZn_2GaO_5$ ($\Delta = 8.4$ K) than in $TmMgGaO_4$ ($\Delta = 5.9$ K [28]). The resulting larger transverse field to exchange interaction ratio places $TmZn_2GaO_5$ closer to the nonmagnetic polarized state [29], thereby suppressing the magnetic ordering. This observation can explain the lower transition temperature in $TmZn_2GaO_5$ (∼0.3 K) compared with $TmMgGaO_4$(∼1 K [23]).

A recent neutron scattering study reported the absence of long-range magnetic order in $TmZn_2GaO_5$ and proposed that it resides in the polarized phase near the boundary with the clock phase [34]. However, our heat capacity measurements reveal a specific heat anomaly consistently in two independent single-crystal samples [Fig. 4(e)&(f)]. This anomaly, together with the observed nonlinear magnetization behavior [Fig. 3(b)], provides direct evidence for a field-induced phase transition, challenging this interpretation. One plausible explanation for the relatively weak magnetic signal is that $TmZn_2GaO_5$ lies within the clock phase but exceptionally close to the phase boundary. In this case, the ordered $z$ components

of the magnetic moments are reduced, and since the $xy$ components present multipolar characters that cannot be directly detected by neutrons [23], the neutron signals would be significantly weaker than in $TmMgGaO_4$. This is consistent with our observations that the transition temperatures are relatively low for $TmZn_2GaO_5$ ($\sim$0.3 K) and the phase-transition-induced heat capacity anomaly is less pronounced. Therefore, detecting magnetic order in $TmZn_2GaO_5$ via neutron diffraction would likely require substantially larger sample volumes and extended counting times. Future neutron studies are essential to reinvestigate the magnetic order in $TmZn_2GaO_5$ and track the field evolution of magnetic ordering. Moreover, it would also be valuable to corroborate our findings with local probes such as nuclear magnetic resonance (NMR) or muon spin relaxation ($\mu$SR), which are more sensitive to weak magnetic ordering.

## CONCLUSIONS

In summary, high-quality $TmZn_2GaO_5$ single crystals were successfully synthesized using the floating zone method. Through magnetization and heat capacity measurements, we established the TFIM on a triangular lattice as the effective low-energy description of this material and obtained the complete field-dependent phase diagram. This diagram indicates the potential realization of BKT transitions and an intermediate BKT phase in zero field, which are replaced with more conventional magnetic order and phase transitions under longitudinal fields. Our findings present a pristine quantum Ising magnet exhibiting long-range order free of observable structural disorder, promising for the study of BKT physics in quantum materials.

## ACKNOWLEDGMENTS

This work was supported by the National Key R&D Program of China (Grant No. 2024YFA1408301, 2021YFA1400300) and the National Natural Science Foundation of China (Grant No. 12574139, 12425403, 11934017, 12261131499). A portion of this work was carried out at the Synergetic Extreme Condition User Facility (SECUF).

[1] Balents L 2010 *Nature* **464** 199–208 ISSN 0028-0836
[2] Zhou Y, Kanoda K and Ng T K 2017 *Reviews of Modern Physics* **89** 025003
[3] Broholm C, Cava R J, Kivelson S A, Nocera D G, Norman M R and Senthil T 2020 *Science* **367** eaay0668
[4] Shen Y, Li Y D, Wo H, Li Y, Shen S, Pan B, Wang Q, Walker H C, Steffens P, Boehm M, Hao Y, Quintero-Castro D L, Harriger L W, Frontzek M D, Hao L, Meng S, Zhang Q, Chen G and Zhao J 2016 *Nature* **540** 559–562 ISSN 0028-0836
[5] Li Y, Adroja D, Biswas P K, Baker P J, Zhang Q, Liu J, Tsirlin A A, Gegenwart P and Zhang Q 2016 *Physical Review Letters* **117** 097201
[6] Paddison J A M, Daum M, Dun Z, Ehlers G, Liu Y, Stone M B, Zhou H and Mourigal M 2017 *Nature Physics* **13** 117–122 ISSN 1745-2473
[7] Shen Y, Li Y D, Walker H C, Steffens P, Boehm M, Zhang X, Shen S, Wo H, Chen G and Zhao J 2018 *Nature Communications* **9** 4138 ISSN 2041-1723
[8] Li Y D, Shen Y, Li Y, Zhao J and Chen G 2018 *Physical Review B* **97** 125105
[9] Dai P L, Zhang G, Xie Y, Duan C, Gao Y, Zhu Z, Feng E, Tao Z, Huang C L, Cao H, Podlesnyak A, Granroth G E, Everett M S, Neuefeind J C, Voneshen D, Wang S, Tan G, Morosan E, Wang X, Lin H Q, Shu L, Chen G, Guo Y, Lu X and Dai P 2021 *Physical Review X* **11** 021044
[10] Xie M, Zhuo W, Cai Y, Zhang Z and Zhang Q 2024 *Chinese Physics Letters* **41** 117505 ISSN 0256-307X
[11] Bag R, Xu S, Sherman N E, Yadav L, Kolesnikov A I, Podlesnyak A A, Choi E S, da Silva I, Moore J E and Haravifard S 2024 *Physical Review Letters* **133** 266703
[12] Wu H C H, Pratt F L, Huddart B M, Chatterjee D, Goddard P A, Singleton J, Prabhakaran D and Blundell S J 2025 *Physical Review Letters* **135** 046704
[13] Zhao L, Chen T, Stone M B, Zhang Q, Sarkis C L, Koohpayeh S M and Broholm C 2025 Quenched disorder in the triangular lattice antiferromagnet $YbZn_2GaO_5$ (*Preprint* 2507.12592)
[14] Gao B, Chen T, Tam D W, Huang C L, Sasmal K, Adroja D T, Ye F, Cao H, Sala G, Stone M B, Baines C, Verezhak J A T, Hu H, Chung J H, Xu X, Cheong S W, Nallaiyan M, Spagna S, Maple M B, Nevidomskyy A H, Morosan E, Chen G and Dai P 2019 *Nature Physics* **15** 1052–1057 ISSN 1745-2481
[15] Sibille R, Gauthier N, Lhotel E, Porée V, Pomjakushin V, Ewings R A, Perring T G, Ollivier J, Wildes A, Ritter C, Hansen T C, Keen D A, Nilsen G J, Keller L, Petit S and Fennell T 2020 *Nature Physics* **16** 546–552 ISSN 1745-2481
[16] Smith E M, Benton O, Yahne D R, Placke B, Schäfer R, Gaudet J, Dudemaine J, Fitterman A, Beare J, Wildes A R, Bhattacharya S, DeLazzer T, Buhariwalla C R C, Butch N P, Movshovich R, Garrett J D, Marjerrison C A, Clancy J P, Kermarrec E, Luke G M, Bianchi A D, Ross K A and Gaulin B D 2022 *Physical Review X* **12** 021015
[17] Porée V, Yan H, Desrochers F, Petit S, Lhotel E, Appel M, Ollivier J, Kim Y B, Nevidomskyy A H and Sibille R 2025 *Nature Physics* **21** 83–88 ISSN 1745-2481
[18] Smith E M, Schäfer R, Dudemaine J, Placke B, Yuan B, Morgan Z, Ye F, Moessner R, Benton O, Bianchi A D and Gaulin B D 2025 *Physical Review X* **15** 021033
[19] Bhardwaj A, Porée V, Yan H, Gauthier N, Lhotel E, Petit S, Quilliam J A, Nevidomskyy A H, Sibille R and Changlani H J 2025 *Physical Review B* **111** 155137
[20] Liu C, Li Y D and Chen G 2018 *Physical Review B* **98** 045119 URL `https://link.aps.org/doi/10.1103/PhysRevB.98.045119`

[21] Zheng S, Gu Y, Gu Y, Kao Z, Wang Q, Wo H, Zhu Y, Liu F, Wu L, Sheng J, Chang J, Ohira-Kawamura S, Murai N, Niedermayer C, Mazzone D G, Chen G and Zhao J 2024 *Physical Review B* **109** 075159

[22] Cevallos F A, Stolze K, Kong T and Cava R J 2018 *Materials Research Bulletin* **105** 154–158 ISSN 0025-5408 URL http://www.sciencedirect.com/science/article/pii/S0025540817339958

[23] Shen Y, Liu C, Qin Y, Shen S, Li Y D, Bewley R, Schneidewind A, Chen G and Zhao J 2019 *Nature Communications* **10** 4530 ISSN 2041-1723 URL https://doi.org/10.1038/s41467-019-12410-3

[24] Qin Y, Shen Y, Liu C, Wo H, Gao Y, Feng Y, Zhang X, Ding G, Gu Y, Wang Q, Shen S, Walker H C, Bewley R, Xu J, Boehm M, Steffens P, Ohira-Kawamura S, Murai N, Schneidewind A, Tong X, Chen G and Zhao J 2022 *Science Bulletin* **67** 38–44 ISSN 2095-9273

[25] Li Y, Bachus S, Deng H, Schmidt W, Thoma H, Hutanu V, Tokiwa Y, Tsirlin A A and Gegenwart P 2020 *Physical Review X* **10** 011007 URL https://link.aps.org/doi/10.1103/PhysRevX.10.011007

[26] Hu Z, Ma Z, Liao Y D, Li H, Ma C, Cui Y, Shangguan Y, Huang Z, Qi Y, Li W, Meng Z Y, Wen J and Yu W 2020 *Nature Communications* **11** 5631 ISSN 2041-1723

[27] Dun Z, Bai X, Paddison J A M, Hollingworth E, Butch N P, Cruz C D, Stone M B, Hong T, Demmel F, Mourigal M and Zhou H 2020 *Physical Review X* **10** 031069

[28] Liu C, Huang C J and Chen G 2020 *Phys. Rev. Res.* **2**(4) 043013 URL https://link.aps.org/doi/10.1103/PhysRevResearch.2.043013

[29] Isakov S V and Moessner R 2003 *Physical Review B* **68** 104409 URL https://link.aps.org/doi/10.1103/PhysRevB.68.104409

[30] Damle K 2015 *Physical Review Letters* **115** 127204 URL https://link.aps.org/doi/10.1103/PhysRevLett.115.127204

[31] Biswas S and Damle K 2018 *Physical Review B* **97** 085114 URL https://link.aps.org/doi/10.1103/PhysRevB.97.085114

[32] Li H, Liao Y D, Chen B B, Zeng X T, Sheng X L, Qi Y, Meng Z Y and Li W 2020 *Nature Communications* **11** 1111 ISSN 2041-1723 URL https://doi.org/10.1038/s41467-020-14907-8

[33] Liao D Y, Li H, Yan Z, Wei H T, Li W, Qi Y and Meng Z Y 2021 *Physical Review B* **103** 104416

[34] Ennis M, Bag R, Cookmeyer T, Stone M B, Kolesnikov A I, Hong T, Balents L and Haravifard S 2025 Emergent hidden multipolar state in the triangular lattice magnet $TmZn_2GaO_5$ (*Preprint* 2503.22009)

[35] Dun Z, Daum M, Baral R, Fischer H E, Cao H, Liu Y, Stone M B, Rodriguez-Rivera J A, Choi E S, Huang Q, Zhou H, Mourigal M and Frandsen B A 2021 *Physical Review B* **103** 064424

[36] Zheng S, Wo H, Gu Y, Luo R L, Gu Y, Zhu Y, Steffens P, Boehm M, Wang Q, Chen G and Zhao J 2023 *Physical Review B* **108** 054435

[37] Chaikin P and Lubensky T 1995 *Press, Cambridge*